Spin-transfer torque switching in magnetic tunnel junctions and spin-transfer torque random access memory

2007 J. Phys.: Condens. Matter 19 165209

(http://iopscience.iop.org/0953-8984/19/16/165209)

IOP PUBLISHING JOURNAL OF PHYSICS: CONDENSED MATTER

J. Phys.: Condens. Matter **19** (2007) 165209 (13pp) doi:10.1088/0953-8984/19/16/165209

Spin-transfer torque switching in magnetic tunnel junctions and spin-transfer torque random access memory

Zhitao Diao, Zhanjie Li, Shengyuang Wang, Yunfei Ding, Alex Panchula, Eugene Chen, Lien-Chang Wang and Yiming Huai

Grandis Incorporated, 1123 Cadillac Court, Milpitas, CA 95035, USA

E-mail: Zhanjie.Li@grandisinc.com

Received 30 June 2006, in final form 26 September 2006
Published 6 April 2007
Online at stacks.iop.org/JPhysCM/19/165209

Abstract

We present experimental and numerical results of current-driven magnetization switching in magnetic tunnel junctions. The experiments show that, for MgO-based magnetic tunnelling junctions, the tunnelling magnetoresistance ratio is as large as 155% and the intrinsic switching current density is as low as 1.1×10^6 A cm^{-2}. The thermal effect and current pulse width on spin-transfer magnetization switching are explored based on the analytical and numerical calculations. Three distinct switching modes, thermal activation, dynamic reversal, and precessional process, are identified within the experimental parameter space. The switching current distribution, write error, and read disturb are discussed based on device design considerations. The challenges and requirements for the successful application of spin-transfer torque as the write scheme in random access memory are addressed.

(Some figures in this article are in colour only in the electronic version)

1. Introduction

Recently, there has been a considerable interest in the phenomenon of spin-polarized current-induced magnetization switching in nano-elements due to its potential application in future high density non-volatile memory devices. When an electron current passes through a ferromagnetic layer, the conduction electron spin is preferentially polarized along the magnetization direction and the current becomes spin polarized. The spin-polarized current, which flows through a second ferromagnetic layer in a spin valve structure or magnetic tunnel junction, exerts a spin torque on the magnetic moment of the magnetic layer due to the interaction between the conduction electron spin and the local magnetization. Since the original prediction of the existence of spin-transfer torque [1, 2], there have been a number of theoretical attempts to understand the microscopic origins [3–12], and various experimental verifications have been

carried out in magnetic nanostructures [13–27]. It is noted that the all different theories, which may be correct within their physical assumptions, offer different views on the mechanism of spin-transfer torque. However, a similar mathematical formula of spin-transfer torque is predicted regardless of the microscopic detail. The reason is that all microscopic approaches are based on rather general arguments: for a system consisting of itinerant electrons and local moments, the total angular momentum is conserved even when the system is out of equilibrium.

Spin-transfer torque generated by a spin current fundamentally differs from the conventional magnetic torque created by an effective magnetic field. Without the spin torque, the magnetic system always seeks a local magnetic energy minimum. However, for the spin torque driven magnetization dynamic process, the spin-polarized current can pump magnetic energy into the magnetic system, such that, when the pumping energy exactly compensates the damping loss energy in a precession cycle, the magnetization motion is in a precessional state [28–31]. When the spin-polarized current reaches a threshold value, i.e., the input energy is larger than the energy loss, the spin current drives the magnetization switching. More interestingly, the temperature dependence of the magnetization switching shows an intriguing relation between thermally activated magnetization reversal and spin torque assisted magnetization reversal in a long current pulse regime [32–36]. In the standard thermal activation process, the magnetization reversal is determined by the classical Boltzmann factor $\exp(-E_b/k_BT)$, where E_b is the energy barrier and T is the temperature. In the presence of the spin torque, it is difficult to define the energy barrier since the spin torque is a non-conservative force and there is no energy associated with the spin torque. However, when the current density is smaller than the critical current density J_{c0} and the magnetic field is smaller than the coercive field, the Néel–Brown's formula $\tau = f_0^{-1}\exp(E_b/k_BT_{eff})$ is still satisfied by introducing an effective temperature $T_{eff} = T(1 - J/J_{c0})^{-1}$ [37, 38], though the above correction to the temperature breaks down at large currents since it is conceptually meaningless to have a negative effective temperature. Furthermore, when $J > J_{c0}$ the precessional state is generated and the precessional state is neither at a local energy minimum nor a maximum. The thermal transition occurs between a static state and a precessional state [39].

The application of spin-transfer torque in MRAM-type (magnetoresistive random access memory) devices requires a number of challenges to be overcome. First, the current density for the spin-transfer torque write is still too high for integration with a CMOS (complementary metal oxide semiconductor) and it is desirable to realize the spin torque write with low switching current density and high tunnelling magnetoresistance (TMR) ratio in magnetic tunnel junctions since a small current helps to decrease the selection transistor size in a 1T-1MTJ (single-transistor, single-magnetic tunnelling junction) design and to increase the reliability of the tunnelling barrier. A high value of TMR is required for fast read access speed. There are several ways to reduce the critical switching current density J_{c0} and these include material parameter optimization as well as structure engineering. The former includes the use of different insulating barriers and free layers with low moment [40] since the threshold current density is primarily governed by the thin-film easy-plane anisotropy $4\pi M_s$, whereas the latter includes the design of film structures to increase the spin transfer efficiency η due to $J_{c0} \propto 1/\eta$ [41]. Second, a present-day CMOS operates at speeds in the gigahertz range. For such a short pulse regime, the switching time is dependent on the current density and initial state of magnetization of the free layers. The achievement of robust switching is of importance in the nanosecond regime in which the current-induced Oersted field is not negligible during the initial stages of switching and onset of precession [42–44]. Finally, by taking advantage of a lower current for magnetization switching, it is of equal importance to ensure an error-free and disturb-free write and read operation by setting sufficient separation between the write and read currents with consideration of integration process variation.

In this paper, we address spin torque write technology, its application in spin-transfer torque random access memory (STT-RAM), and related device design considerations, which are all closely associated with the underlying physics of the spin-transfer torque effect and dynamic process. This paper is organized as follows. In section 2, we describe current reduction schemes including both material and structure engineering. In section 3, we discuss the thermal effect on current-driven magnetization switching based on analytical and numerical calculations. In section 4, we present device design consideration for STT-RAM such as write current distribution, write error and read disturb, and insulating barrier reliability; this is followed by a brief conclusion in section 5.

2. Current density reduction scheme

2.1. Materials engineering

In general, the critical current density J_{c0} is a good measure of current-driven magnetization switching in a nanomagnetic device.

$$J_{c0} = \frac{2e\alpha M_s t_F (H_K \pm H_{ext} + 2\pi M_s)}{\hbar \eta} \tag{1}$$

where e is the electron charge, α is the damping constant, M_s is the saturation magnetization, t_F is the thickness of the free layer, $\hbar$ is the reduced Planck's constant, H_{ext} is the external field, H_K is the effective anisotropy field including magnetocrystalline anisotropy and shape anisotropy, and η is the spin transfer efficiency.

Equation (1) gives a current density threshold. When $J > J_{c0}$, an initial stable magnetization state of the free layer along the easy axis becomes unstable at zero temperature and the magnetization enters a stable precessional state or a complete reversal occurs. At a finite temperature, thermal agitation plays an important role in reducing the switching current at long current pulses,

$$J_c = J_{c0}\left(1 - \frac{k_B T}{K_F V} \ln \frac{t_p}{\tau_0}\right) \tag{2}$$

where τ_0 is the relaxation time and t_p is the current pulse width. From equation (2), one can estimate the critical current density J_{c0} by extrapolating the experimentally observed switching current density J_c at $t_p = \tau_0$.

With materials engineering, as seen from equation (1), the critical current density J_{c0} can be reduced by using materials with a low magnetization M_s and/or a high spin transfer efficiency η. Recent experiments showed that CoFeB is one of the most promising candidates for this purpose. For a typical $CoFe_{10}$ alloy, the magnetization value is 1540 emu cm^{-3}, whereas the magnetization of $Co_{40}Fe_{20}B_{20}$ is less than 1050 emu cm^{-3}, depending on the layer thickness. A rough estimate from equation (1) shows a reduction in J_{c0} by a factor of about 2, assuming the other parameters remain unchanged. On the other hand, the magnetic tunnel junction is an important vehicle in reducing current density since it provides a high polarization as well as a tunable resistance–area product (RA) value. By using a crystalline MgO layer instead of amorphous AlO_x, the TMR increases from 30–70% to 300% [47, 48] at room temperature. The critical current density J_{c0} is expected to be lowered by about two times due to much higher spin polarization.

A typical field hysteresis loop (R–H) and a current loop (R–I) are shown in figures 1(a) and (b) for an MTJ cell with an AlO_x barrier; and in figures 2(a) and (b) for an MgO–MTJ cell. The magnetic tunnel junction films used were of

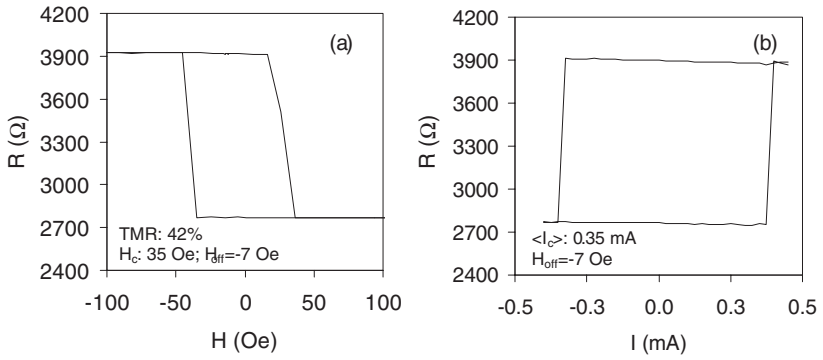

Figure 1. The field hysteresis loop (a) and current loop (b) in an AlO_x–MTJ cell. The nominal cell dimension is 127×148 nm^2 and the average critical current density $\langle J_{c0} \rangle = 6 \times 10^6$ A cm^{-2} [45].

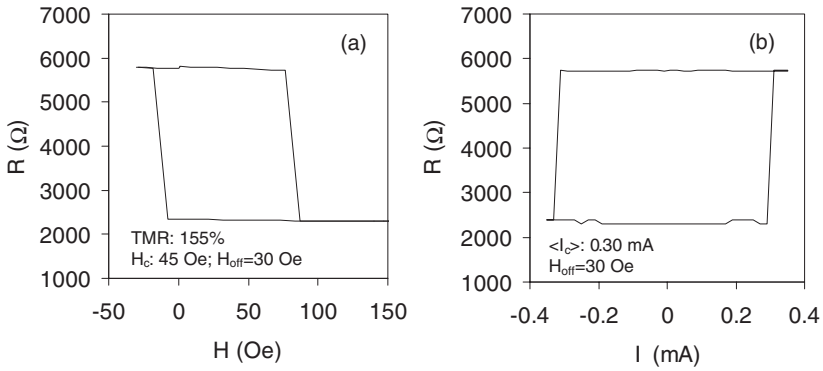

Figure 2. The field hysteresis loop (a) and current loop (b) in a MgO–MTJ cell. The nominal cell dimension is 125×220 nm^2 and the average critical current density $\langle J_{c0} \rangle = 2.2 \times 10^6$ A cm^{-2} [45].

the form Ta(3)/PtMn(20)/CoFe(2)/Ru(0.7)/CoFeB(2)/AlO_x/CoFeB(2.5)/Ta(3) (nm) and Ta(5)/PtMn(20)/CoFe(2)/Ru(0.8)/CoFeB(2)/MgO/CoFeB(2.5)/Ta(8) (nm). The MTJ films were subsequently patterned into deep submicrometre elliptical-shaped pillars. A quasistatic tester with pulse current capability was used to measure the resistance as a function of magnetic field and current at room temperature. The offset field $H_{\rm off}$, experienced by the free layers due to the orange-peel coupling field and the dipolar field from the adjacent pinned layers, was balanced by applying an external field $H_{\rm a} = H_{\rm off}$ during switching current measurements.

For an AlO_x–MTJ, the nominal magnetic cell dimension is 127 nm $\times$ 148 nm and the TMR is 42% with RA $\approx$ 40 Ω μm^2. The average switching current $\langle I_{\rm c} \rangle$ is 0.35 mA at a pulse width of 30 ms at room temperature, where $\langle I_{\rm c} \rangle = (|I_{\rm c}^{\rm P\to AP}| + |I_{\rm c}^{\rm AP\to P}|)/2$ and $I_{\rm c}^{\rm P\to AP}(I_{\rm c}^{\rm AP\to P})$ is the switching current from a parallel (anti-parallel) to an anti-parallel (parallel) state, the average critical current density is about 6×10^6 A cm^{-2}. For a MgO–MTJ whose cell dimension is 125 nm $\times$ 220 nm and TMR is about 155% with RA $\approx$ 50 Ω μm^2, $J_{\rm c0}$ is found to be 2.2×10^6 A cm^{-2}, which is about one third of that in AlO_x MTJS [45]. The observed critical current density $J_{\rm c0}$ in the MgO based MTJ is the lowest value reported in single MTJ based structures.

2.2. Structure improvement

In MTJ structures consisting of one pinned and one free layer, the spin torque is exerted on the magnetization of the free layer when a current flows through this structure. It is a straightforward concept to put a second pinned layer on the other side of the free layer, separated by an insulating layer [46].

For an MTJ cell with a dual structure consisting of two MgO barriers, the average switching current density at the pulse width of 30 ms was achieved of 0.52×10^6 A cm^{-2} at room temperature and the RA is about 100 Ω μm^2. The critical current density J_{c0} is found to be 1.1×10^6 A cm^{-2}. Compared to the single pinned layer MgO–MTJ, the dual structure leads to a reduction in J_{c0} by a factor of 2.0. To date, this critical current density of 1.1×10^6 A cm^{-2} is the lowest achieved by the way of structure improvement.

3. Current-driven magnetization switching modes

In an MTJ structure, the dynamics of the free layer magnetization is determined by the standard Landau–Lifshitz–Gilbert (LLG) equation with the addition of a spin-transfer torque,

$$\frac{\partial \mathbf{m}}{\partial t} = -\gamma \mathbf{m} \times (\mathbf{H}_{\text{eff}} + \mathbf{h}_{\text{th}}) + \alpha \mathbf{m} \times \frac{\partial \mathbf{m}}{\partial t} + \frac{\gamma \hbar J \eta(\mathbf{m}, \mathbf{m}_{\text{p}})}{2e M_{\text{s}} t_{\text{F}}} \mathbf{m} \times (\mathbf{m} \times \mathbf{m}_{\text{p}}) \tag{3}$$

where $\mathbf{m}$ is the reduced magnetization, γ is the gyromagnetic ratio, $\mathbf{m}_{\text{p}}$ is the unit vector along the magnetization of the pinned layer, J is the current density, and $\eta(\mathbf{m}, \mathbf{m}_{\text{p}})$ describes the angular dependence of the efficiency of the spin torque, and its detailed formula is model dependent. For simplicity, we assume that $\eta(\mathbf{m}, \mathbf{m}_{\text{p}})$ is a constant in our following discussion. $\mathbf{h}_{\text{th}}$ is the thermal random field that is assumed to be an independent Gaussian random function with zero mean and no correlation. $\mathbf{H}_{\text{eff}}$ is the effective field that consists of the external field, the anisotropy field, the magnetostatic field, the current-induced Oersted field and the exchange coupling field,

$$\mathbf{H}_{\text{eff}} = \mathbf{H}_{\text{ext}} + \mathbf{H}_K + \mathbf{H}_{\text{stat}} + \mathbf{H}_{\text{Oersted}} + \frac{2A}{M_{\text{s}}} \nabla^2 \mathbf{m} \tag{4}$$

where A is the exchange stiffness constant.

Before discussing our full micromagnetic simulation, we present some insights into the current-driven magnetization switching based on a macro-spin model. In the macro-spin model, the free layer is assumed to be a single domain, and the effective field is simplified as $\mathbf{H}_{\text{eff}} = H_{\text{ext}}\mathbf{e}_x + H_K \mathbf{e}_x - 4\pi M_{\text{s}} m_z \mathbf{e}_z$. With a set of material parameters $\alpha = 0.02$, $H_K = 500$ Oe and the demagnetization factor $4\pi M_{\text{s}} = 18\,000$ Oe, the global picture of current-driven magnetization switching is shown in figure 3 based on analytical and numerical calculations. Upon varying the current pulse widths, three distinct switching modes have been found: thermal activation (solid line), dynamic reversal (dotted line) and precessional switching (thick solid line). We describe each of these switching modes below.

3.1. Thermal activation

For a long current pulse, the magnetization switching is a thermally activated process. The magnetization switching probability is shown in figure 4 with a small current $J = 0.75 J_{c0}$. If the temperature remains unchanged during the switching process, the switching probabilities are exactly the same, and the initial thermal distributions are irrelevant, whereas, with two different temperatures during the switching process, the probability is strikingly different even with the same initial conditions. It is found from figure 4 that, in the thermal activation regime, the magnetization switching is independent of the initial conditions and is only determined

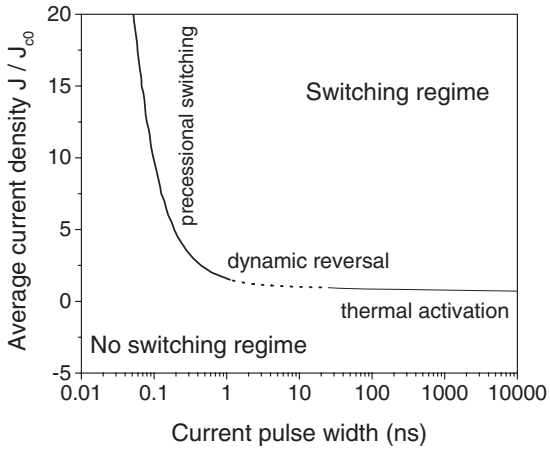

Figure 3. Spin current driven magnetization switching phase diagram. The three switching modes are thermal activation (solid line), dynamic reversal (dotted line) and precessional switching (thick solid line). The parameters are taken as $\alpha = 0.02$, $H_K = 500$ Oe and $4\pi M_s = 18$ kOe.

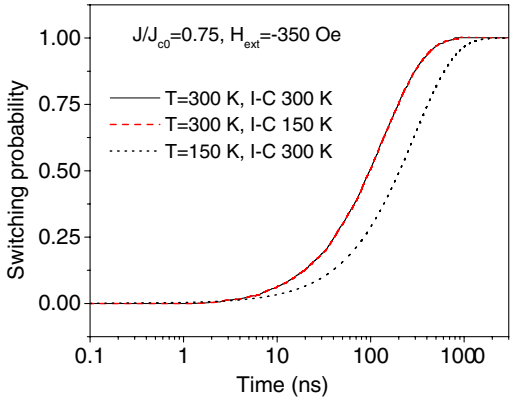

Figure 4. The switching probability in the thermal activation regime. The external field is $H_{ext} = -350$ Oe and the current density is $J = 0.75 J_{c0}$. A total of 100 000 samples are taken in our macro-spin model calculations. The other parameters are the same as those in figure 3.

by thermal agitation during the switching process. The thermal switching probability $P(t_p)$ is fitted exactly by the Néel–Brown relaxation formula $P(t_p) = 1 - \exp(-t_p/\tau)$, where t_p is the pulse width, and the relaxation time is modified as $\tau = f_0^{-1} \exp(E_b/k_B T_{eff})$ in the presence of spin torque [33, 37, 38], $T_{eff} = T(1 - J/J_{c0})^{-1}$. The modified Néel–Brown formula works well for long current pulses but it breaks down for short and intermediate current pulses.

3.2. Precessional switching

With a very short current pulse, the magnetization switching is mainly dependent on the initial thermal distribution. The magnetization switching distribution and switching probability are shown in figures 5(a) and (b) for a large current $J = 5J_{c0}$. We found that with the same initial condition ($T = 300$ K) the switching distribution and probability are almost unchanged under different thermal agitations during the switching process. As shown in

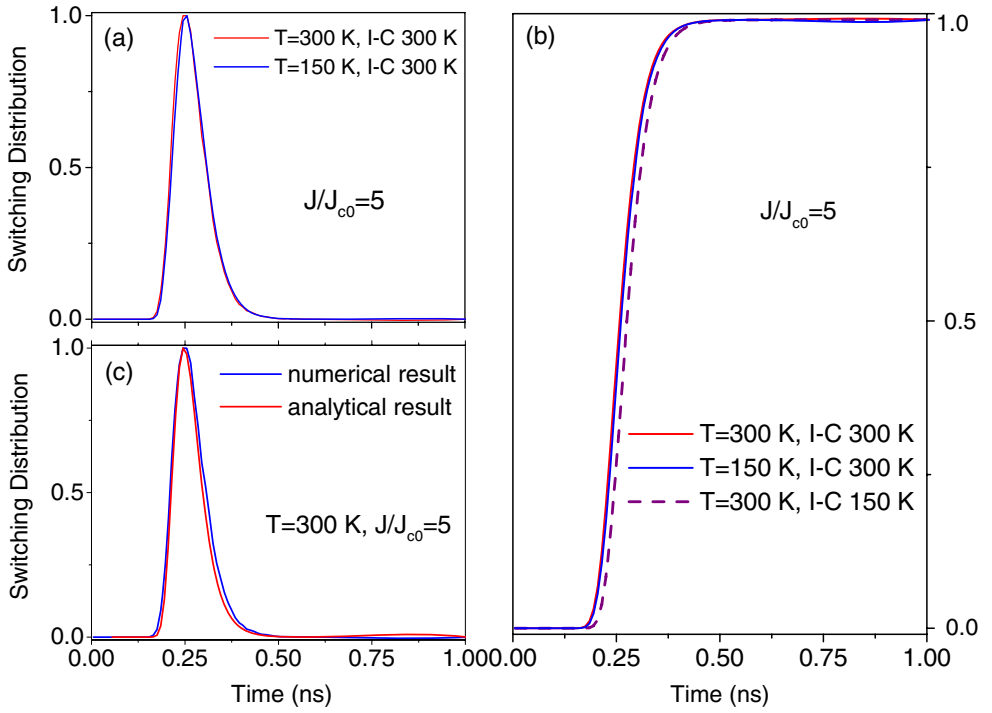

Figure 5. (a) The switching distributions with the same initial condition and the different temperatures during the switching process for a given large current $J = 5.0J_{c0}$. (b) The switching probability with different initial conditions and different temperatures during process. (c) The analytical and numerical switching distributions.

figure 5(b) the switching probability is shifted with different initial conditions but with the same thermal agitation. It is found that in the precessional switching regime, the magnetization reversal is almost independent of the thermal agitation during the switching process. One can obtain an approximate estimation of the switching time at zero temperature [28], $t_p \propto (J - J_{c0})^{-1} \ln(\pi/2\theta)$, θ being the initial angle between the magnetization vector and the easy axis. At finite temperature, θ is a thermal distribution. To illustrate the precessional switching process with a thermal disturbance, the switching distribution is estimated to be as long as $J \gg J_{c0}$,

$$P(t_p) \propto \exp\left(\frac{H_K M_s V}{2k_B T}(1 - \cos^2\phi)\right)(J - J_{c0})\sin^2\phi$$
$$\phi = \frac{\pi}{2}\exp\left(-\frac{\eta\mu_B}{eM_s t_F}(J - J_{c0})t_p\right) \tag{5}$$

where use has been made of the fact that $2\pi M_s^2 \gg H_K M_s \gg k_B T/V$. The magnetization switching distribution obtained from the equation above is in agreement with the numerical result shown in figure 5(c) for $J = 5J_{c0}$.

3.3. Dynamic reversal

The most interesting switching mode is the dynamic reversal at intermediate current pulses, which corresponds to the operating speed of practical STT-RAM. One immediately notices

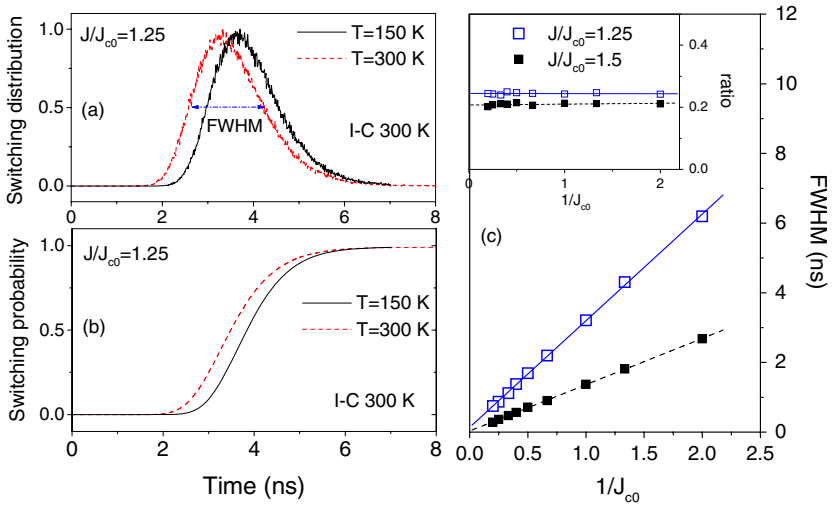

Figure 6. The switching distribution (a) and the switching probability (b) in the intermediate pulse regime with the same initial condition and different temperatures during the switching process. (c) The full width at half maximum and the ratio $2\sigma_t$ (inset) for different currents.

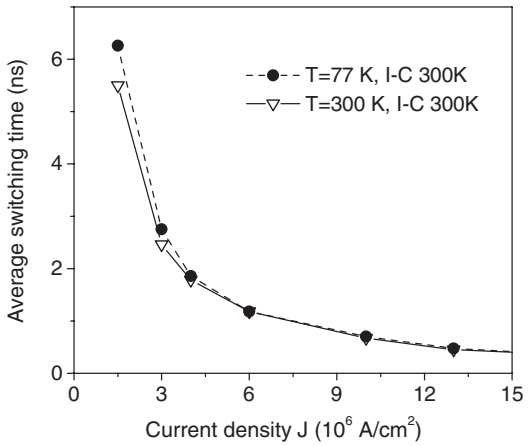

Figure 7. The average switching time as a function of current density based on full micromagnetic simulation. The parameter are taken as $\alpha = 0.01$, $H_k = 5$ Oe and the effective demagnetization field 2800 Oe (see footnote 1). The average switching time is statistically obtained from an ensemble of 60 switching events.

from figure 3 that the dynamic reversal occurs in a small range. For the same initial thermal condition, the magnetization switching distribution and probability are shifted with different temperatures during the switching process, as shown in figures 6(a) and 7(b). It is found that the magnetization reversal is determined both by the initial thermal distribution and the thermal agitation during the switching process. The dynamic reversal is a combination of precessional and thermally activated switching in the nanosecond regime. Unlike dealing with either of these two regimes, it is difficult to obtain an explicit formula to describe the switching distribution/probability due to the complicated reversal process.

The full width at half maximum (FWHM) Δt of the switching distribution is an important factor in the potential application of STT-RAM. For an intermediate current width, the FWHM is approximately proportional to $1/J_{c0}$ and weakly dependent on the thermal factor $K_F V/k_B T$, which is different from that in a thermally activated process. We plot Δt in figure 6(c) with two currents $J = 1.25J_{c0}$ and $J = 1.5J_{c0}$. With increasing current density J, Δt decreases; however, the ratio of the FWHM to the average switching time $2\sigma_t = \Delta t/t_{ave}$ is almost a constant, as shown in the inset of figure 6(c).

Beyond the macro-spin model, a full micromagnetic modelling is required to completely understand the magnetization switching in the presence of current. First, the free layer may not behave as a single uniform domain due to the shape anisotropy. Second, the effect of the current-induced Oersted field on the magnetization vectors at the sample centre is much different from that at edge. In our micromagnetic simulation, an elliptical-shaped free layer is used with a size of 160 nm × 90 nm and a thickness of 2.5 nm. The material parameters are taken as the damping constant $\alpha = 0.01$, the magnetocrystalline anisotropy field of 5 Oe, the stiffness constant $A = 1.4 \times 10^{-11}$ J m^{-1} and the effective demagnetization field of 2800 Oe.[1] With the parameters specified above, we begin our simulation by laterally dividing the free layer into an $N \times N$ grid with a grid spacing $D = 5.0$ nm.

In the short and intermediate pulse width regimes, we restudy the thermal effect on the magnetization dynamics. The average switching time versus current density is shown in figure 7 with the same initial thermal distribution ($T = 300$ K). Under different thermal agitations at 300 and 77 K, in the short pulse regime ($t_p \leqslant 1.5$ ns), the magnetization switching is a precessional process, and it is almost independent of the thermal agitation and determined by the initial condition. In the intermediate pulse regime, the magnetization reversal depends both on the initial condition and the thermal agitation. The micromagnetic results are consistent with the macro-spin model even though two sets of different material parameters were used.

4. Design considerations

4.1. Write current distribution

As shown in section 3, at long current pulses, magnetization switching driven by spin currents is a thermally activated process, and the distribution is primarily sensitive to the thermal factor of the free layer in the MTJ cells. The cumulative probability distribution is determined by the modified Néel–Brown relaxation formula, which is asymmetric, and the low current tail is much wider than the high current tail [49]. As a result, a small change in the maximum writing current results in a low write error. However, the read current has to be further away from the peak to achieve the same error rate. This intrinsic asymmetry is detrimental to the read disturb margin; and small read current is beneficial from the point of view of potential dielectric break-down in the junction and therefore reliability.

A tight distribution of critical current is required to reduce read disturb and write errors and thereby improve the write reliability. While the within-die critical current distribution depends on the cell geometry and material property distributions, the within-cell distribution is shown to be closely related to the thermal stability of the magnetic cell. The implication of current distribution and thermal stability of bits is discussed both in terms of the stability of memory cells in the idle state as well as the behaviour of memory cell during read/write operations.

[1] In some MTJ structures, it is found that the free layers have a large perpendicular anisotropy H_{per} along the z axis. Thus, the effective demagnetization field is $\mathbf{H}_d = (4\pi M_s - H_{per})\mathbf{e}_z$. This results in reducing the intrinsic critical current $J_{c0} = 2e\alpha M_s t_F(H_K \pm H_{ext} + 2\pi M_s - H_{per}/2)/\hbar\eta$.

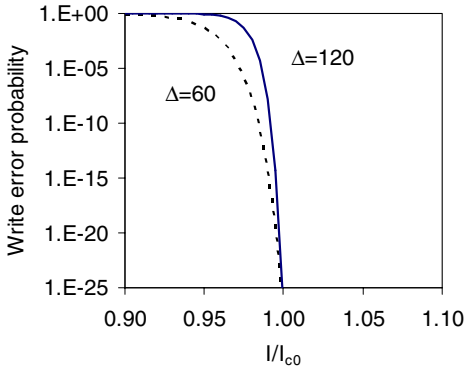

Figure 8. The write error probability as a function of current for the two different thermal factors $\Delta = 60$ (dotted line) and 120 (solid line) for a pulse width of 60 ns.

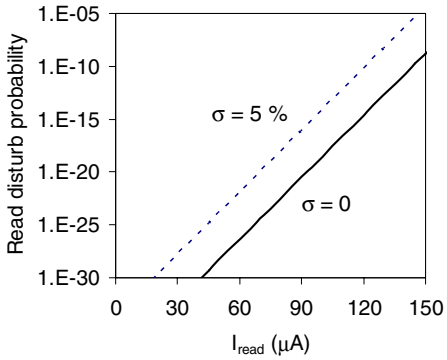

Figure 9. The read disturb probability as function of read current I_{read} at a pulse width of 10 ns with the median critical current of 200 μA.

4.2. Write error and read disturb

In the STT-RAM architecture the same transistor is used to both read and write the magnetic bit by passing current through the magnetic tunnel junction. A high current of appropriate polarity is used to change the magnetic state of the bit, while a low current is used to read the bit. The use of the same method, with different amplitudes, for reading and writing creates two types of error: write error and read disturb. Write errors occur when an insufficient current is passed through the MTJ and the state is not written correctly. Read disturb errors are caused by reading current unintentionally disturbing or writing the bit.

The switching current distribution effect on write error as well as read disturb is further detailed using plots in figures 8 and 9, respectively. Write error is related to the operating margin between writing a high resistance bit and breakdown voltage. Read error is related to the margin in operating current between read and write operation. In figure 8, the write error was estimated by the fraction of an ensemble of magnetic moments that is switched at a particular current and plotted for a pulse width of 60 ns. At this high speed write with small pulse width, a small margin over the median critical current is required to get a very low write error of 10^{-25} when the thermal activation factor is large enough. The margin can be narrowed to 5% from 10% when the $K_{\text{F}}V/k_{\text{B}}T$ increases from 60 to 120. Note that at high speed write (pulse width less than 100 ns) the median critical current remains almost the same, irrespective

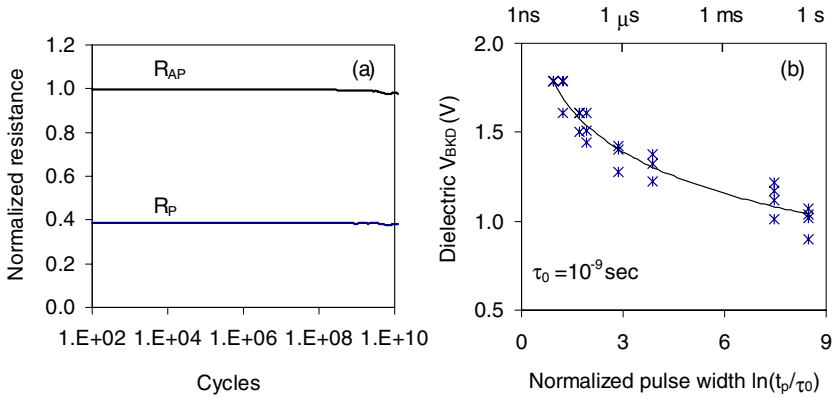

Figure 10. (a) The reliability of the insulating barrier in an MgO–MTJ with 700 mV pulses of 40 ns; (b) the dielectric breakdown voltage as a function of the pulse width.

of the variation of thermal activation factor, while at low speed write it depends significantly on the variation of $K_F V/k_B T$, as does the margin over the median critical current.

In figure 9, the read disturb is represented by cumulative probability distribution between 0 and a read current at a pulse width of 10 ns with the median critical current of 200 μA. To achieve low read disturb, i.e. accidental writing of a bit while trying to read the bit, the read current has to be much smaller than the median critical current. For a read disturbance error rate of 10^{-23}, as seen from figure 9, the thermal factor $\Delta = K_F V/k_B T$ should be larger than 90, and the read current can be 70 μA or about 0.35 times the median critical current. The high $K_F V/k_B T$ implies a narrower critical current distribution and hence increases the margin for error-free operation during read and write cycles. For the benefit of the thermal stability of the stored bit, a $K_F V/k_B T$ value greater than 65 is desirable to get long-term data retention time of >10 years. However, the thermal budget becomes much tighter once the margin for error-free operation during read and write is considered. Since the within-die critical current distribution depends on the cell geometry and material property distributions, the distribution of this kind in the median critical current shown in figure 9 increases the read disturb probability as multiple bits read disturb. Assuming that all other parameters remain the same but with $\sigma = 5\%$ in the median critical current, the read disturb probability is increased by several orders of magnitude at a specified read current. With $K_F V/k_B T \sim 90$, the read current has to be reduced to 50 μA or about 0.25 times the median critical current to maintain the same level of read disturbance error rate. Note that reducing the pulse width has a marginal effect on the read disturb. Maintaining a large enough median critical current, reducing process variation and getting reasonable thermal activation factor contribute most to a well-controlled read disturb during read and write cycles.

4.3. Insulating barrier reliability

The reliability of the insulating barrier in an MgO–MTJ structure was tested with 700 mV pulse of 40 ns as shown in figure 10(a). Cycling of 10^{10} is obtained without intrinsic dielectric breakdown of the barrier or appreciable changes in the parallel and antiparallel resistance states. The test was terminated due to tester and hardware limitations. The results show that the insulating barrier of the MgO–MTJ does not have reliability problem due to dielectric breakdown during write and read cycling. In figure 10(b), the dielectric breakdown voltage is plotted as a function of the pulse width applied. At a long pulse width of about 0.3 s,

the dielectric breakdown voltage is about 1200 mV, close to the value obtained from a DC measurement. It increases almost linearly with decrease in pulse width down to 1 μs, and increases at a still rapid rate in the nanosecond regime to about 1800 mV. In the simplest way, the cycling stress is proportional to pulse width t_p and temperature rise in the device. One expects that a decrease in pulse width directly reduces the electrical stress with smaller diffusion or structure relaxation time. At a high frequency pulse, however, the temperature effect will be suppressed. On the other hand, the diffusion barrier energy responsible for dielectric breakdown is seemingly significantly affected and enlarged at high frequency pulses, implying an increased breakdown voltage as observed in the experiment. From the design point of view, this is beneficial because it widens the margin for write operation and therefore improves device reliability.

5. Conclusions

In summary, we achieved spin current-driven magnetization switching at room temperature with a critical current density J_{c0} as low as 1.1×10^6 A cm^{-2} in MgO based dual MTJ structures. Additional benefits of these structures in terms of critical current density reduction can be achieved by further materials optimization, including the use of new free layer materials to reduce the demagnetization factor or the use of material systems to reduce damping constant. This would help realize the final goal of 10^5 A cm^{-2} critical current density that would be suitable for device application.

We also showed the three magnetization switching modes in the presence of spin current: (a) thermal activation in the long current pulse width regime; (b) dynamic reversal with an intermediate current pulse; (c) precessional switching in the very short pulse width regime. In particular, at the intermediate pulse regime that closely associated to high speed memory device application, both the thermal activation and the precessional mode play significant roles in determining the spin transfer torque-induced magnetization switching.

Finally, we addressed the spin transfer write–read scheme for advanced STT-RAM devices. The margin for both read and write operation is influenced by the thermal factor for long and intermediate current pulses, because of its effect on the switching current distribution. To get sufficient separation between read current, write current and the barrier breakdown current, a tight distribution of the write current is needed. Thus, a high thermal factor $K_F V/k_B T$ is required for both read and write reliability, as well as for long-term retention of the written data.

Acknowledgments

We thank Dmytro Apalkov, Alexander Driskill-Smith, Kiyoshi Kawabata (Renesas Technology), Shufeng Zhang for valuable discussions. This material is based upon work supported by the National Science Foundation under Grant No. 0538973.

References

[1] Slonczewski J C 1996 *J. Magn. Magn. Mater.* **159** L1
[2] Berger L 1996 *Phys. Rev.* B **54** 9359
[3] Slonczewski J C 2002 *J. Magn. Magn. Mater.* **247** 324
Slonczewski J C 2005 *Phys. Rev.* B **71** 024411
[4] Waintal X, Myers E B, Brouwer P W and Ralph D C 2000 *Phys. Rev.* B **62** 12317
[5] Hernando D H, Nazarov1 Yu V, Brataas A and Bauer G E W 2000 *Phys. Rev.* B **62** 5700

[6] Stiles M D and Zangwill A 2002 *Phys. Rev.* B **66** 014407
Stiles M D and Zangwill A 2002 *J. Appl. Phys.* **91** 6812
[7] Wegrowe J-E 2000 *Phys. Rev.* B **62** 1067
[8] Heide C 2001 *Phys. Rev. Lett.* **87** 197201
[9] Zhang S, Levy P M and Fert A 2002 *Phys. Rev. Lett.* **88** 236601
[10] Yang Z and Zhang S 2007 *10th Joint MMM/Intermag Conf. FD-07 (Baltimore, Maryland, USA)*
[11] Levy P M and Fert A 2006 *Phys. Rev. Lett.* **97** 097205
[12] Theodonis I, Kioussis N, Kalitsov A, Chshiev M and Butler W 2006 *Preprint* cond-mat/0606080
[13] Wegrowe J-E, Kelly D, Jaccard Y, Guittienne Ph and Ansermet J-Ph 1999 *Europhys. Lett.* **45** 626
[14] Katine J A, Albert F J, Buhrman R A, Myers E B and Ralph D C 2000 *Phys. Rev. Lett.* **84** 3149
[15] Grollier J, Cros V, Hamzic A, George J M, Jaffres, Fert A, Faini G, Ben Y J and Legall H 2001 *Appl. Phys. Lett.* **78** 3663
[16] Özyilmaz B, Kent A D, Sun J Z, Rooks M J and Koch R H 2004 *Phys. Rev. Lett.* **93** 176604
[17] Tsoi M, Sun J Z and Parkin S S P 2004 *Phys. Rev. Lett.* **93** 036602
[18] Covington M, AlHajDarwish M, Ding Y, Gokemeijer N J and Seigler M A 2004 *Phys. Rev.* B **69** 184406
[19] Mangin S, Ravelosona D, Katine J A, Carey M J, Terris B D and Fullerton E E 2006 *Nat. Mater.* **5** 210
[20] Krivorotov I N, Emley N C, Sankey J C, Kiselev S I, Ralph D C and Buhrman R A 2005 *Science* **307** 228
[21] Ji Y, Chien C L and Stiles M D 2003 *Phys. Rev. Lett.* **90** 106601
[22] Rippard W H, Pufall M R, Kaka S, Russek S E and Silva T J 2004 *Phys. Rev. Lett.* **92** 027201
[23] Sun J Z 1999 *J. Magn. Magn. Mater.* **202** 157
[24] Huai Y, Albert F, Nguyen P, Pakala M and Valet T 2004 *Appl. Phys. Lett.* **84** 3118
Diao Z, Apalkov D, Pakala M, Panchula A, Ding Y and Huai Y 2005 *Appl. Phys. Lett.* **87** 232502
Huai Y, Pakala M, Diao Z and Ding Y 2005 *Appl. Phys. Lett.* **87** 222510
[25] Fuchs G D, Emley N C, Krivorotov I N, Braganca P M, Ryan E M, Kiselev S I, Sankey J C, Ralph D C, Buhrman R A and Katine J A 2004 *Appl. Phys. Lett.* **85** 1205
[26] Tulapurkar A A, Suzuki Y, Fukushima, Kubota H, Maehara H, Tsunekawa K, Djayaprawira D D, Watanabe N and Yuasa S 2005 *Nature* **438** 339
[27] Chiba D, Sato Y, Kita T, Matsukura F and Ohno H 2004 *Phys. Rev. Lett.* **93** 216602
[28] Sun J Z 2000 *Phys. Rev.* B **62** 570
[29] Li Z and Zhang S 2003 *Phys. Rev.* B **68** 024404
[30] Xi H and Lin Z 2004 *Phys. Rev.* B **70** 092403
[31] Bertotti G, Serpico C, Mayergoyz I D, Magni A, d'Aquino M and Bonin R 2005 *Phys. Rev. Lett.* **94** 127206
[32] Urazhdin S, Birge N O, Pratt W P Jr and Bass J 2003 *Phys. Rev. Lett.* **91** 146803
[33] Koch R H, Katine J A and Sun J Z 2004 *Phys. Rev. Lett.* **92** 088302
[34] Myers E B, Albert F J, Sankey J C, Bonet E, Buhrman R A and Ralph D C 2002 *Phys. Rev. Lett.* **89** 196801
[35] Fábián A, Terrier C, Guisan S S, Hoffer X, Dubey M, Gravier L, Ansermet J-Ph and Wegrowe J-E 2003 *Phys. Rev. Lett.* **91** 257209
[36] Pufall M R, Rippard W H, Kaka S, Russek S E, Silva T J, Katine J and Carey M 2004 *Phys. Rev.* B **93** 166603
[37] Li Z and Zhang S 2004 *Phys. Rev.* B **69** 134416
[38] Apalkov D M and Visscher P B 2005 *Phys. Rev.* B **72** 180405
[39] Li Z, He J and Zhang S 2005 *Phys. Rev.* B **72** 212411
[40] Yagami K, Tulapurkar A A, Fukushima A and Suzuki Y 2004 *Appl. Phys. Lett.* **85** 5634
[41] Diao Z, Pakala M, Panchula A, Ding Y, Apalkov D, Wang L-C, Chen E and Huai Y 2006 *J. Appl. Phys.* **99** 08G510
Huai Y, Pakala M, Diao Z and Ding Y 2005 *IEEE Trans. Magn.* **41** 2641
Maass W and Huai Y 2005 *Semicond. Int.* (March)
[42] Lee K-J, Deac A, Redon O, Nozières J-P and Dieny B 2004 *Nat. Mater.* **3** 877
[43] Zhu J-G and Zhu X 2004 *IEEE Trans. Magn.* **40** 182
[44] Apalkov D, Pakala M and Huai Y 2006 *J. Appl. Phys.* **99** 08B907
[45] Huai Y, Apalkov D, Diao Z, Ding Y, Panchula A, Pakala M, Wang L-C and Chen E 2006 *Japan. J. Appl. Phys.* **45** 3835
[46] Huai Y *et al* 2002 *US Patent Specification* 6958927 (9-Oct-2002)
Valet T 2004 *US Patent Specification* 7057921 (11-May-2004)
[47] Parkin S S P, Kaiser C, Panchula A, Rice P M, Hughes B, Samant M and Yang S-H 2004 *Nat. Mater.* **3** 862
[48] Yuasa S, Nagahama T, Fukushima A, Suzuki Y and Ando K 2004 *Nat. Mater.* **3** 868
[49] Pakala M, Huai Y, Valet T, Ding Y and Diao Z 2005 *J. Appl. Phys.* **98** 056107